

Electronic Supplementary Information for

**Isostructural organic binary-host frameworks with
tuneable and diversely decorated inclusion cavities**

Judit Galcera^{1,2}, Tomislav Friščić², Katarzyna E. Hejczyk², László Fábián³, Stuart M. Clark², Graeme M. Day², Elies Molins¹ and William Jones²

¹ Institut de Ciència de Materials de Barcelona (ICMAB-CSIC),
Campus de la UAB, 08193 Bellaterra, Spain
*Email: judit.galcera@gmail.com

² Department of Chemistry, University of Cambridge,
Lensfield Road, Cambridge CB21EW, United Kingdom
*Email: wj10@cam.ac.uk

³ School of Pharmacy, University of East Anglia,
Norwich, NR4 7TJ, United Kingdom

Table of Contents

Section 1 Powder X-ray Diffraction patterns of LAG synthesized compounds (S1-S4)
Section 2 Single Crystal and powder X-ray Diffraction structure studies (S5-S18)
Section 3 Infrared spectroscopy (S19-S22)
Section 4 Thermal Analyses (S23-S25)
Section 5 Computational methods (S26-S27)

Section 1. Powder X-ray Diffraction patterns of LAG synthesized compounds

Powder X-ray diffraction (PXRD) data for the most of the samples was collected on a Philips X'Pert Pro diffractometer using $\text{CuK}\alpha$ radiation ($\lambda = 1.5418 \text{ \AA}$) at 40 kV and 40 mA. Each sample was analyzed between 5 and 40 $^{\circ}2\theta$ at a scan rate of $0.06^{\circ} 2\theta \text{ s}^{-1}$. PXRD data for some of the samples was collected on a Siemens D5000 powder diffractometer using $\text{Cu K}\alpha$ radiation ($\lambda = 1.5406 \text{ \AA}$) at 40 kV and 35 mA. These samples were scanned between 5° and 50° of 2θ , at a scan rate of $0.02^{\circ} 2\theta \text{ s}^{-1}$.

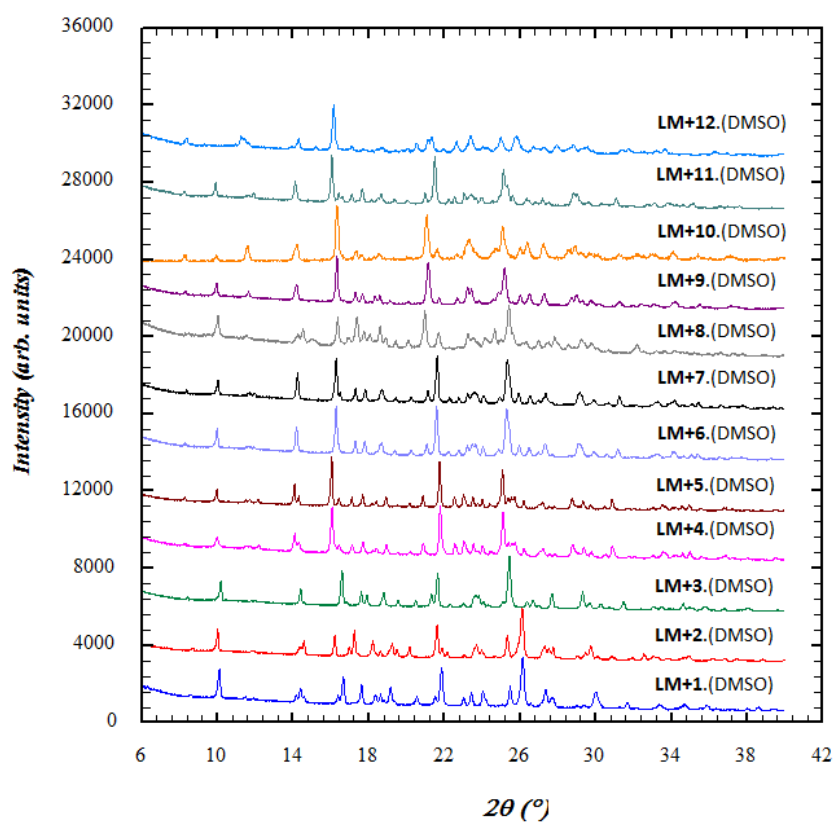


Figure S1. PXRD patterns of the isostructural **LM+DC(guest)** compounds **LM+1.(DMSO)**, **LM+2.(DMSO)**, **LM+3.(DMSO)**, **LM+4.(DMSO)**, **LM+5.(DMSO)**, **LM+6.(DMSO)**, **LM+7.(DMSO)**, **LM+8.(DMSO)**, **LM+9.(DMSO)**, **LM+10.(DMSO)**, **LM+11.(DMSO)** and **LM+12.(DMSO)** obtained by LAG experiments with DMSO as the guest solvent molecule.

Section 1 Powder X-ray Diffraction patterns of LAG synthesized compounds

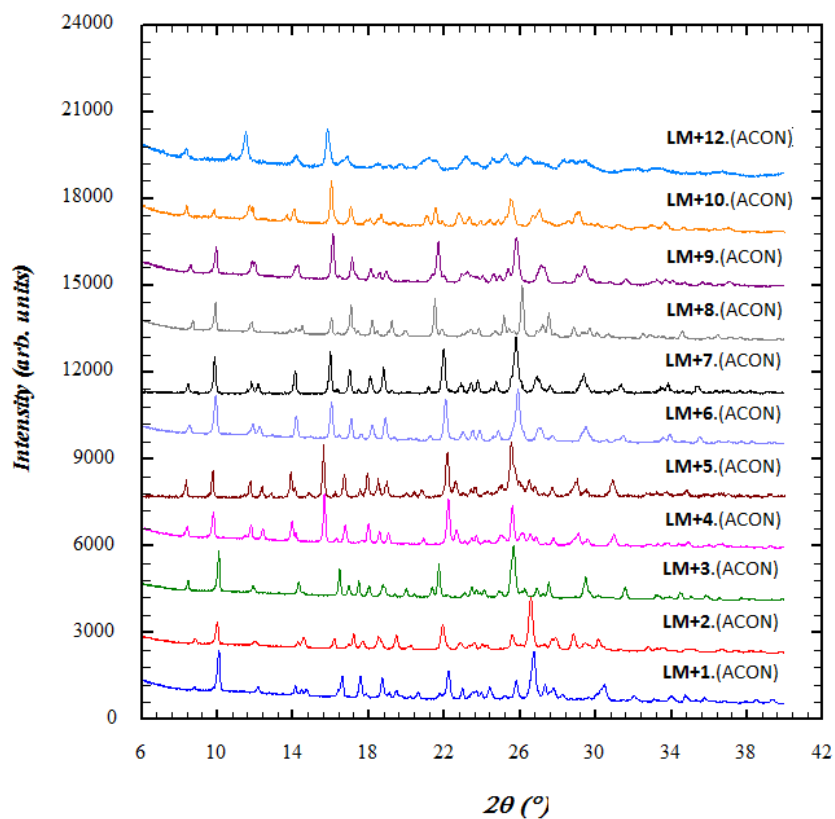


Figure S2. PXRD patterns of the isostructural **LM+DC(guest)** compounds **LM+1.(ACON)**, **LM+2.(ACON)**, **LM+3.(ACON)**, **LM+4.(ACON)**, **LM+5.(ACON)**, **LM+6.(ACON)**, **LM+7.(ACON)**, **LM+8.(ACON)**, **LM+9.(ACON)**, **LM+10.(ACON)** and **LM+12.(ACON)** obtained by LAG experiments with ACON as the guest solvent molecule.

Section 1 Powder X-ray Diffraction patterns of LAG synthesized compounds

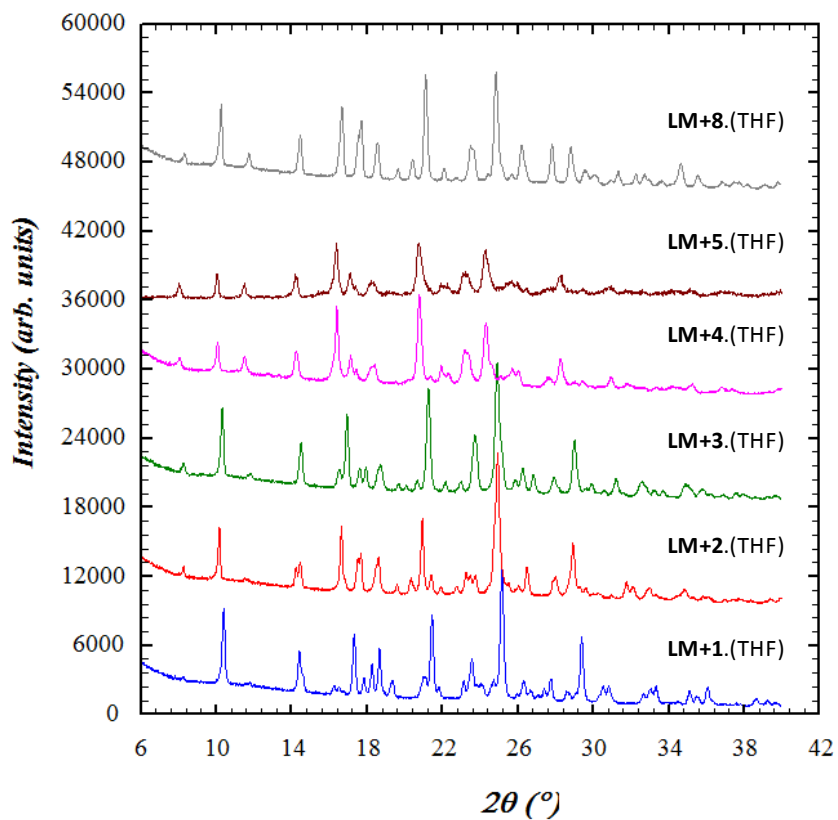


Figure S3. PXRD patterns of the isostructural **LM+DC(guest)** compounds **LM+1.(THF)**, **LM+2.(THF)**, **LM+3.(THF)**, **LM+4.(THF)** and **LM+5.(THF)** obtained by LAG experiments with THF as the guest solvent molecule.

Section 1 Powder X-ray Diffraction patterns of LAG synthesized compounds

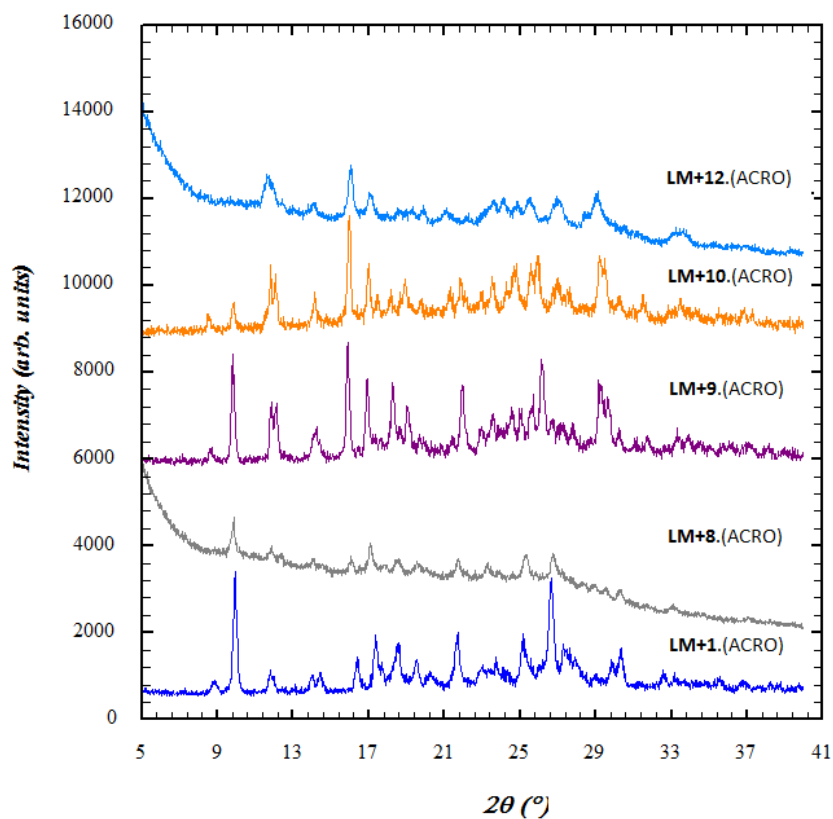


Figure S4. PXRD patterns of the isostructural **LM+DC**.(guest) compounds **LM+1**.(ACRO), **LM+8**.(ACRO), **LM+9**.(ACRO), **LM+10**.(ACRO) and **LM+12**.(ACRO) obtained by LAG experiments with ACRO as the guest solvent molecule.

Section 2. Single Crystal X-ray Diffraction Studies

Single-crystal X-ray diffraction (SCXRD) data were collected at 180(2) K with a Nonius Kappa CCD diffractometer using Mo K α radiation ($\lambda = 0.71073 \text{ \AA}$) at 40 kV and 40 mA and equipped with an Oxford Cryosystems cryostream. Data obtained were processed with the WinGX integrated system software package for SCXRD data solution, refinement, and analysis¹. Crystal structures of all compounds were solved either by direct methods using SHELXS-97² or by charge flipping algorithm using SUPERFLIP³. All the structures were refined by full-matrix least-squares refinement on F^2 using SHELXL-97². Anisotropic model was used the refinement of all the non-hydrogen atoms. In general the hydrogen atoms were introduced in calculated positions and refined as riding on their bonded atoms with idealized geometries and with restrained isotropic displacement parameters. In some cases, when the N-H and OH hydrogen atoms were located from the difference Fourier maps showing a reasonable geometry and bonding distances, the hydrogen atom positions were introduced as determined from the data. Solvent disorder model was adopted for all the structures containing DMSO as the solvent molecule. The sulphur atom appears as disordered into two positions with variable final refined occupation factors depending on the structure. In the case of **LM+2.(DMSO)** the DMSO solvent molecule shows disorder into two positions with final refined occupancies of 0.65 and 0.35. In the case of **LM+3.(DMSO)** the DMSO solvent molecule shows disorder into two positions with final refined occupancies of 0.60 and 0.40. In the case of **LM+4.(DMSO)** the two independent DMSO solvent molecules show disorder into two positions with final refined occupancies of 0.95-0.05 and 0.79-0.21. In this case the sulfur atom of one of the DMSO molecules was refined anisotropically by using the SIMU and ISOR restraints in SHELX. In the case of **LM+5.(DMSO)** one of the two independent DMSO solvent molecules shows disorder into two positions with final refined occupancies of 0.78-0.22. In the case of **LM+6.(DMSO)** the two independent DMSO solvent molecules show disorder into two positions with final refined occupancies of 0.90-0.10 and 0.57-0.43. In the case of **LM+9.(DMSO)** the DMSO solvent molecule shows disorder into two positions with final refined occupancies of 0.65 and 0.35. In the case of **LM+1.(DMSO-THF)** a solvent disorder model was adopted by introducing a DMSO molecule and a THF molecule with respective refined occupation factors of 0.20 and 0.80. In the structure **LM+1.(THF)** the THF solvent molecule shows a disordered into two positions with final refined occupancies of 0.75 and 0.25. The disorder of the THF molecule was modelled using a SAME instruction restraint in SHELX. The disordered atoms were modelled as anisotropic by using an EADP restraint. In the case of the **LM+4.(ACON)** a disorder model has been adopted for one of the acetone solvent molecules. The acetone solvent

Section 2 Single Crystal X-ray and Powder Diffraction Structural Studies

molecule shows a disordered into two positions with final refined occupancies of 0.52 and 0.48. The disorder of the acetone molecule was modelled using a SAME instruction restraint in SHELX. The disordered atoms were modelled as anisotropic by using and EADP restraint.

In the refinement of the **LM+10**.(ACON) a disorder model of the entire ACON molecule into two positions with one half of occupation was used. In the final refinement cycles of the **LM+8**.(ACON) structure a residual positive electron density peak of $1.3 \text{ e.}\text{\AA}^{-3}$ was found and a disorder model was adopted by introducing nitromethane molecule with an occupation factor of one half. This disorder model with a cavity occupied with one half of ACON and one half of nitromethane provided the best refinement parameters without important residual density peaks (note that the single crystal used for the SCXRD data collection was grown from a mixture of nitromethane and acetone solvents). The crystal structures presented were examined using PLATON⁴ and Mercury CSD 2.2⁵ software. Note that for the structures **LM+4**.(DMSO), **LM+4**.(ACON), **LM+5**.(DMSO), **LM+6**.(DMSO) the PLATON⁴ suggests a possible pseudo centre of symmetry in the model. However, a center of symmetry is not compatible with the known chirality of the dicarboxylic acids that constitute these structures (D-tartaric acid, L-tartaric acid and D-malic acid). On the other hand, in the soft synthesis conditions used, racemization is not expected. As the acids used as reactives in the synthesis are known to be chiral forms, the structures of the salts were solved in the non-centrosymmetric chiral space group $P2_1$.

In the cases of guest-free collapsed **LM+3** and **LM+2**, the final difference Fourier maps showed residual electron density peaks. In order to account for the residual electron density a disorder model of the LM molecule was adopted. Both structures were successfully refined with a disorder of the LM into two positions, showing two different conformations of the dichlorophenyl rings which rotate approximately 180° . The final refinement parameters improved considerably and the residual density peaks were reduced to reasonable values. A similar type of disorder has also been previously reported in a LM analogue⁶ and it is also consistent with other unpublished own data on LM structures. The final refined occupation factors of the two disordered LM are 0.94-0.06 in **LM+3** and 0.93-0.07 in **LM+2**. In some other cases the final difference Fourier maps also showed some residual density peaks that may correspond to this type of disorder, but attempts to model it using similarity restraints were unsuccessful. Note that for **LM+2** various attempts to growth bigger and better quality crystals were made by using different solvents, but the crystals obtained were either solvated forms or small weakly diffracting crystals. The data set used for crystal structure solution presented was the best we could obtain from a weakly diffracting crystal. While the data completeness is low, the crystal structure solution and refinement results obtained are reasonable with standard R factor values and the structure obtained for **LM+2** is also consistent with the structure of the isostructural related compound **LM+3**.

Section 2 Single Crystal X-ray and Powder Diffraction Structural Studies

The **LM+9**.(DMSO) crystallizes in the monoclinic space group $P 2_1/c$. The asymmetric unit contains one LM molecule, one-half of a *D,L*-chlorosuccinic acid molecule, which is located on an inversion center, and one DMSO solvent molecule. Therefore, both enantiomers are included in the structure, being a racemic salt of *D,L*-chlorosuccinic acid with 50 % of L-type enantiomer and 50% of D-type enantiomer in the structure. The same situation occurs for **LM+10**.(ACON), that crystallizes in the monoclinic space group $P 2_1/c$. The asymmetric unit contains one LM molecule, one-half of a *D,L*-bromosuccinic acid molecule, which is located on an inversion center, and one DMSO solvent molecule, being a racemic salt of *D,L*-bromosuccinic acid with 50 % of L-type enantiomer and 50% of D-type enantiomer in the structure. In both cases a disorder model of the central carbons into two different positions was attempted by using various restraints, but the refinement was unstable and finally the positions were fixed by using EADP and EXYZ restraints. Note that for both structures **LM+9**.(DMSO) and **LM+10**.(ACON) several attempts to grow better crystals were made and different data collection sets with different crystals were evaluated, but most of the crystals grown were either too small or of poor quality.

1. Farrugia, L. J. J. WinGX suite for small-molecule single-crystal crystallography. *Appl. Crystallogr.* 1999, **32**, 837–838 (1999)
2. Sheldrick, G. M. A short history of SHELX. *Acta Crystallogr. Sec.A* **64**, 112–122 (2008)
3. Palatinus, L., Chapuis G. Superflip - a computer program for the solution of crystal structures by charge flipping in arbitrary dimensions. *J. Appl. Cryst.* **40**, 786-790 (2007)
4. A.L.Spek PLATON, A Multipurpose Crystallographic Tool. Utrecht University, Utrecht, The Netherlands (2005).
5. Mercury CSD 2.2. Cambridge Crystallographic Data Centre, Cambridge, UK.
6. Janes, R., 3,5-Diamino-6-(2-fluorophenyl)-1,2,4-triazine-dimethylformamide (1/1). *Acta Crystallographica Section C* **2000**, 56 (3), 362-364.

Table S5. Unit cell parameters determined by SCXRD for the isostructural **LM+DC**.(guest) compounds.

SCXRD reference compound	Unit cell parameters				
	<i>a</i>	<i>b</i>	<i>c</i>	β	Volume
LM+1 .(THF)	11.2006(3)	10.2189(2)	16.3395(5)	109.043(1)	1767.84 (8)
LM+2 .(DMSO)	10.6601(2)	10.9576(2)	15.8831(3)	108.768(1)	1756.64(6)
LM+3 .(DMSO)	11.0200(2)	10.6723(2)	15.9451(3)	108.840(1)	1774.81(6)
LM+3 .(ACON)	10.8143(3)	10.7320(3)	16.0105(4)	108.560(1)	1761.52(8)
LM+4 .(DMSO)	11.0958(1)	11.0374(2)	15.6848(2)	106.947(1)	1837.48(4)
LM+4 .(ACON)	10.7524(2)	11.3284(2)	15.5321(3)	105.024(1)	1827.25(6)
LM+5 .(DMSO)	11.0961(1)	11.0420(1)	15.6858(2)	106.950(1)	1838.39(3)
LM+6 .(DMSO)	11.0150(2)	10.8376(2)	15.9178(3)	108.111(1)	1806.06(6)
LM+8 .(ACON)	10.6172(2)	10.9788(2)	15.9940(4)	109.129(1)	1761.38(6)
LM+9 .(DMSO)	11.0489(3)	10.8220(4)	16.2310(7)	109.403(2)	1830.53(12)
LM+10 .(ACON)	10.7610(3)	11.0390(4)	16.0900(6)	107.284(2)	1825.03(11)

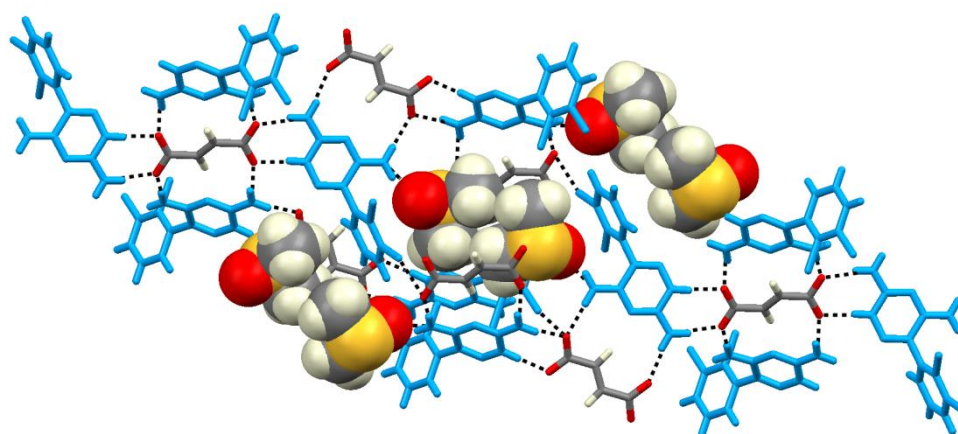


Figure S6. The crystal packing diagram of **LM+2**.(DMSO) structure showing the two main hydrogen-bonded ring synthons of type $R_2^2(8)$ and $R_2^2(13)$ between the **LM** (in blue) and **2** molecules. The DMSO guest molecules (drawn in spacefill mode) are filling the cavities limited by the dichlorophenyl and triazine groups of the **LM** and the central carbon backbone of the acid **2**.

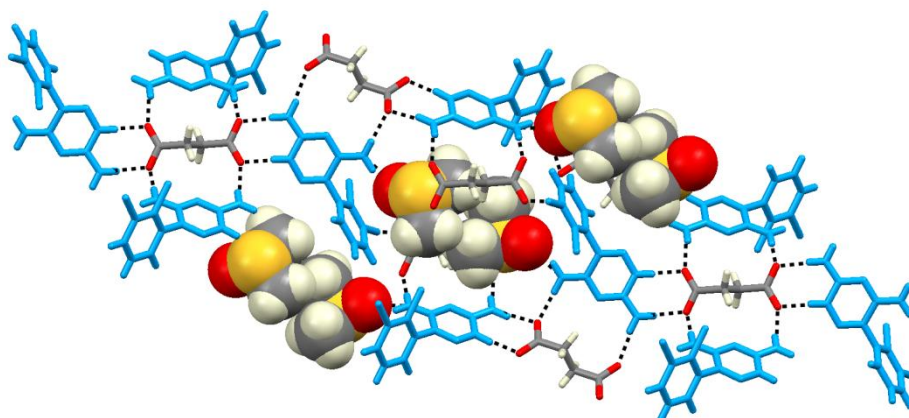


Figure S7. The crystal packing diagram of **LM+3**.(DMSO) structure showing the two main hydrogen-bonded ring synthons of type $R_2^2(8)$ and $R_2^2(13)$ between the **LM** (in blue) and **3** molecules. The DMSO guest molecules (drawn in spacefill mode) are filling the cavities limited by the dichlorophenyl and triazine groups of the **LM** and the central carbon backbone of the acid **3**.

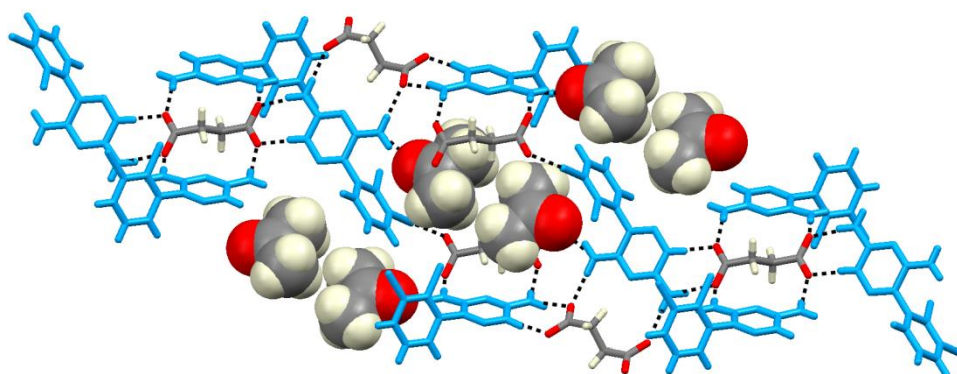


Figure S8. The crystal packing diagram of **LM+3**.(ACON) structure showing the two main hydrogen-bonded ring synthons of type $R_2^2(8)$ and $R_2^2(13)$ between the **LM** (in blue) and **3** molecules. The ACON guest molecules (drawn in spacefill mode) are filling the cavities limited by the dichlorophenyl and triazine groups of the **LM** and the central carbon backbone of the acid **3**.

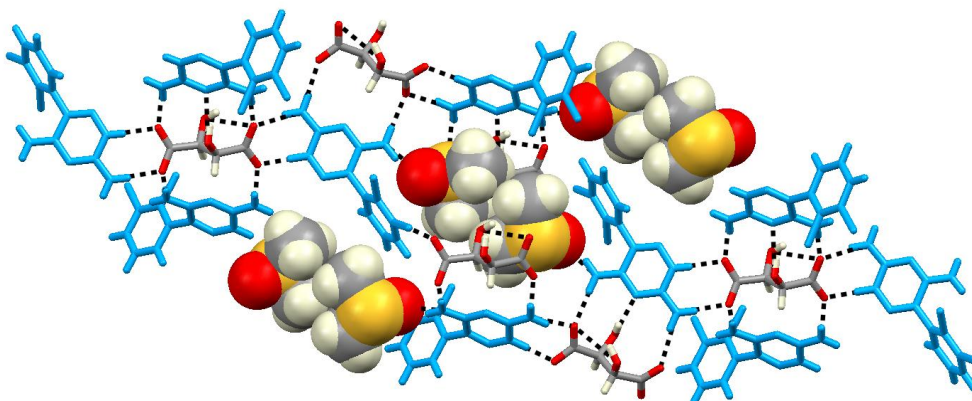


Figure S9. The crystal packing diagram of **LM+4**.(DMSO) structure showing the two main hydrogen-bonded ring synthons of type $R_2^2(8)$ and $R_2^2(13)$ between the **LM** (in blue) and **4** molecules. The DMSO guest molecules (drawn in spacefill mode) are filling the cavities limited by the dichlorophenyl and triazine groups of the **LM** and the central carbon backbone of the acid **4**.

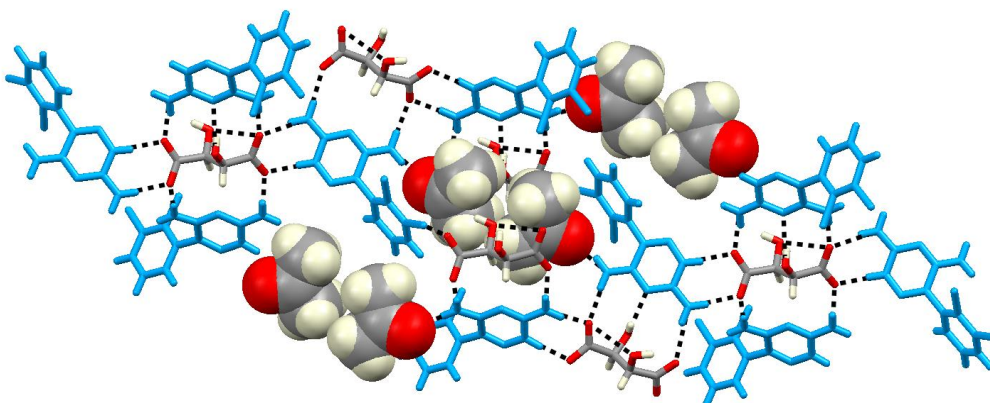


Figure S10. The crystal packing diagram of **LM+4**.(ACON) structure showing the two main hydrogen-bonded ring synthons of type $R_2^2(8)$ and $R_2^2(13)$ between the **LM** (in blue) and **4** molecules. The ACON guest molecules (drawn in spacefill mode) are filling the cavities limited by the dichlorophenyl and triazine groups of the **LM** and the central carbon backbone of the acid **4**.

Section 2 Single Crystal X-ray and Powder Diffraction Structural Studies

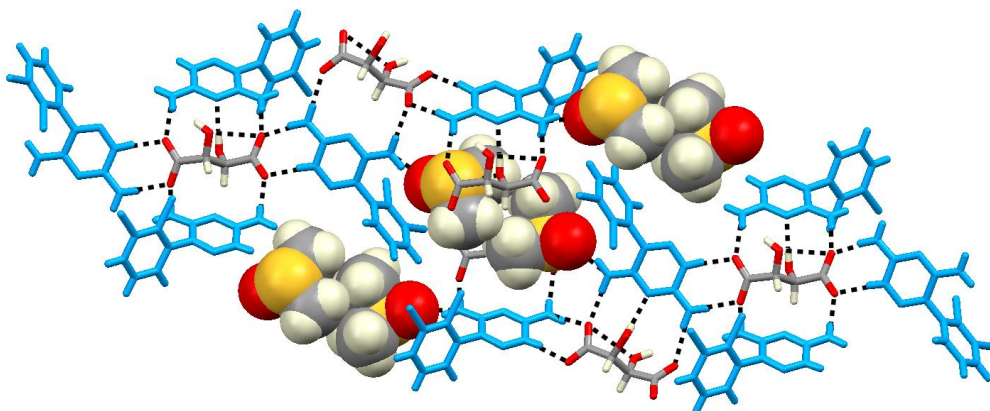


Figure S11. The crystal packing diagram of **LM+5**.(DMSO) structure showing the two main hydrogen-bonded ring synthons of type $R_2^2(8)$ and $R_2^2(13)$ between the **LM** (in blue) and **5** molecules. The DMSO guest molecules (drawn in spacefill mode) are filling the cavities limited by the dichlorophenyl and triazine groups of the **LM** and the central carbon backbone of the acid **5**.

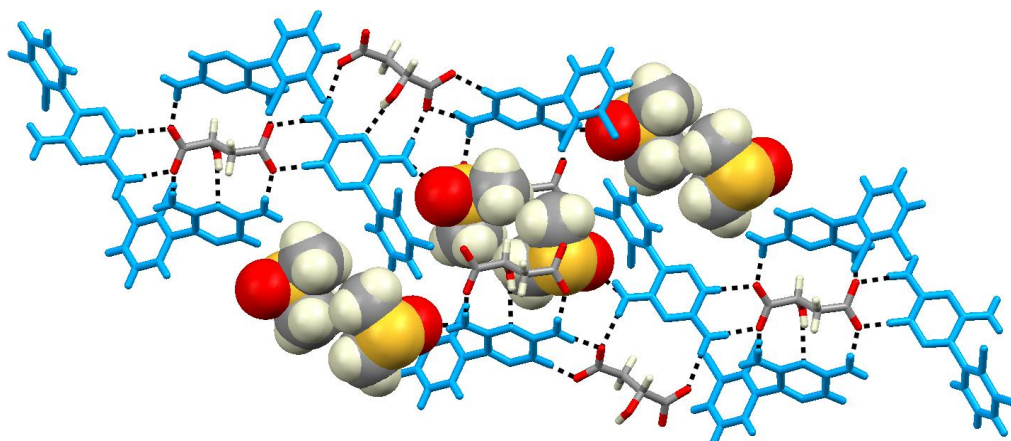


Figure S12. The crystal packing diagram of **LM+6**.(DMSO) structure showing the two main hydrogen-bonded ring synthons of type $R_2^2(8)$ and $R_2^2(13)$ between the **LM** (in blue) and **6** molecules. The DMSO guest molecules (drawn in spacefill mode) are filling the cavities limited by the dichlorophenyl and triazine groups of the **LM** and the central carbon backbone of the acid **6**.

Section 2 Single Crystal X-ray and Powder Diffraction Structural Studies

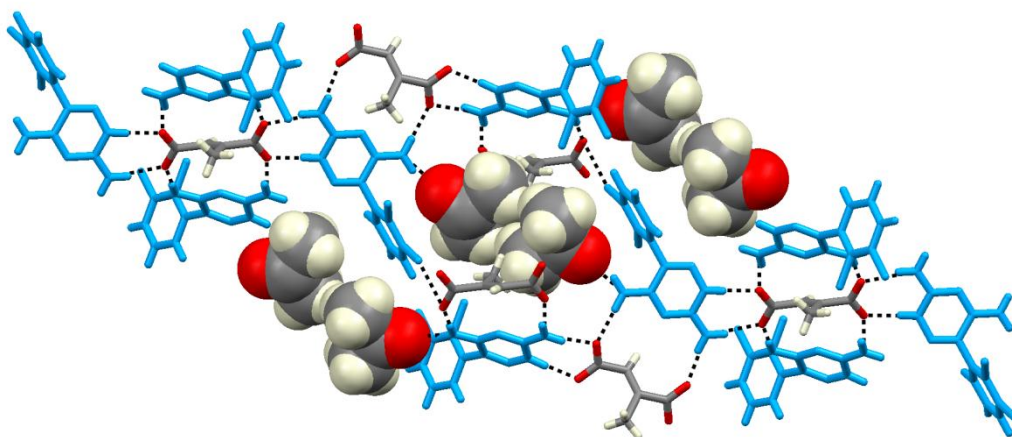


Figure S13. The crystal packing diagram of **LM+8**.(ACON) structure showing the two main hydrogen-bonded ring synthons of type $R_2^2(8)$ and $R_2^2(13)$ between the **LM** (in blue) and **8** molecules. The ACON guest molecules (drawn in spacefill mode) are filling the cavities limited by the dichlorophenyl and triazine groups of the **LM** and the central carbon backbone of the acid **8**.

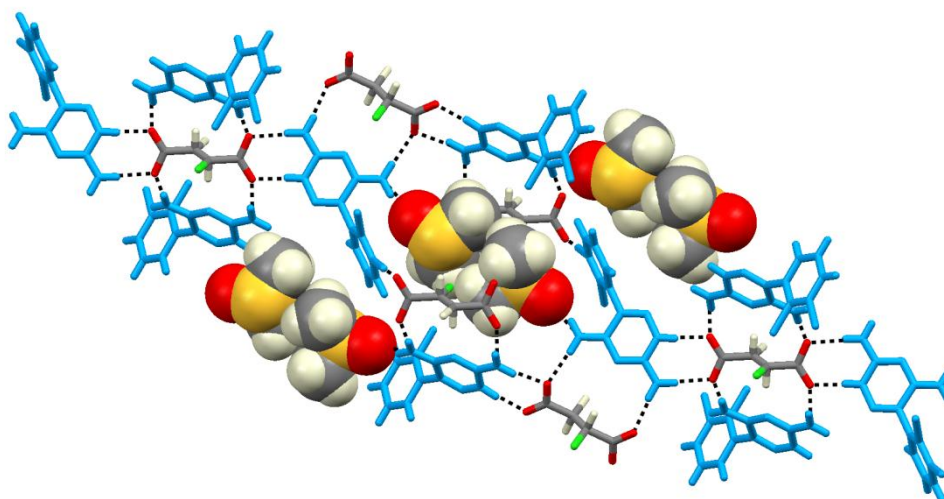


Figure S14. The crystal packing diagram of **LM+9**.(DMSO) structure showing the two main hydrogen-bonded ring synthons of type $R_2^2(8)$ and $R_2^2(13)$ between the **LM** (in blue) and **9** molecules. The DMSO guest molecules (drawn in spacefill mode) are filling the cavities limited by the dichlorophenyl and triazine groups of the **LM** and the central carbon backbone of the acid **9**.

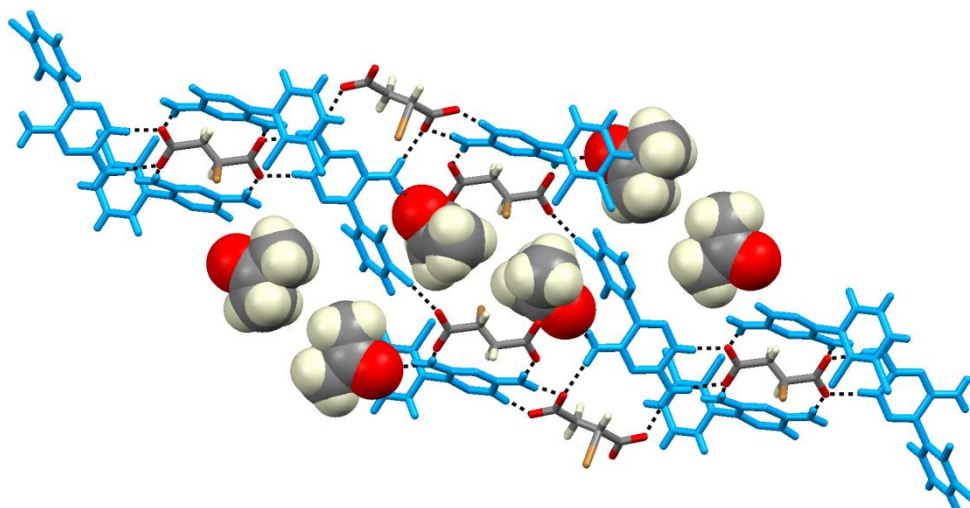


Figure S15. The crystal packing diagram of **LM+10.(ACON)** structure showing the two main hydrogen-bonded ring synthons of type $R_2^2(8)$ and $R_2^2(13)$ between the **LM** (in blue) and **10** molecules. The ACON guest molecules (drawn in spacefill mode) are filling the cavities limited by the dichlorophenyl and triazine groups of the **LM** and the central carbon backbone of the acid **10**.

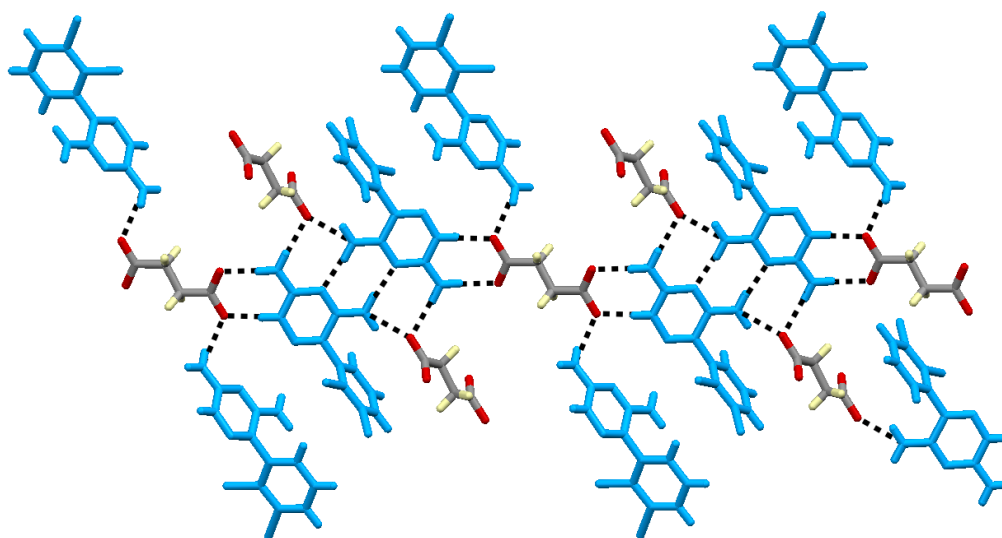


Figure S16. The crystal packing diagram of the collapsed **LM+3** structure showing hydrogen-bonded heterosynthons of type $R_2^2(8)$ between the **DC** and **LM**(blue) and homosynthons of type $R_2^2(8)$ between pairs of **LM** molecules. The remaining N-H groups of **LM** are additionally interacting by bifurcated hydrogen bonds to neighbouring carboxylates.

Crystal structure determination from synchrotron powder X-ray diffraction

PXRD data used for crystal structure solution of **LM+12**.(ACON) was collected at the Diamond Synchrotron beamline I11 using a radiation wavelength of 1.06237 Å and at a temperature of 293K. The data were processed with the DASH⁶ integrated software package for PXRD structure solution. An initial background subtraction was performed to eliminate the background contribution attributed to sample damage caused by synchrotron radiation exposure during the data collection. The PXRD pattern was indexed with DICVOL06⁷ and intensities were extracted by Palwey⁸ refinement. Crystal structure solution was obtained by simulated annealing. Two solutions, which differed only in the orientation of the anion, gave similar fit to the observed PXRD pattern. A final model was created by combining the two solutions and assuming disorder of the two orientations. The crystal structure was refined by Rietveld refinement using the EXPGUI⁹ interface to the GSAS¹⁰ software. All atoms were modelled with a common isotropic displacement factor. Bond lengths and angles were restrained to values taken from the single crystal structure of the DL stereoisomer. The final refined occupation factors for the two orientations of the anion are 0.48 and 0.52. Figure S17 shows the difference between the final Rietveld refined calculated PXRD and the experimentally observed PXRD.

1. DASH: W.I.F David, K. Shankland, J. van de Streek, E. Pidcock, W.D.S. Motherwell, J.C. Cole, *J. Appl. Cryst.*, 2006, 39, 910-915.
2. DICVOL06: D. Louer, A. Boultif, *Z. Kristallogr. Suppl.*, 2007, 26, 191-196.
3. GSAS: A.C. Larson, R.B. von Dreele, *General Structure Analysis System (GSAS)*, Los Alamos National Laboratory Report, LAUR 86-748, 2004.
4. EXPGUI: B. H. Toby, *J. Appl. Cryst.*, 2001, 34, 210-221.

Section 2 Single Crystal X-ray and Powder Diffraction Structural Studies

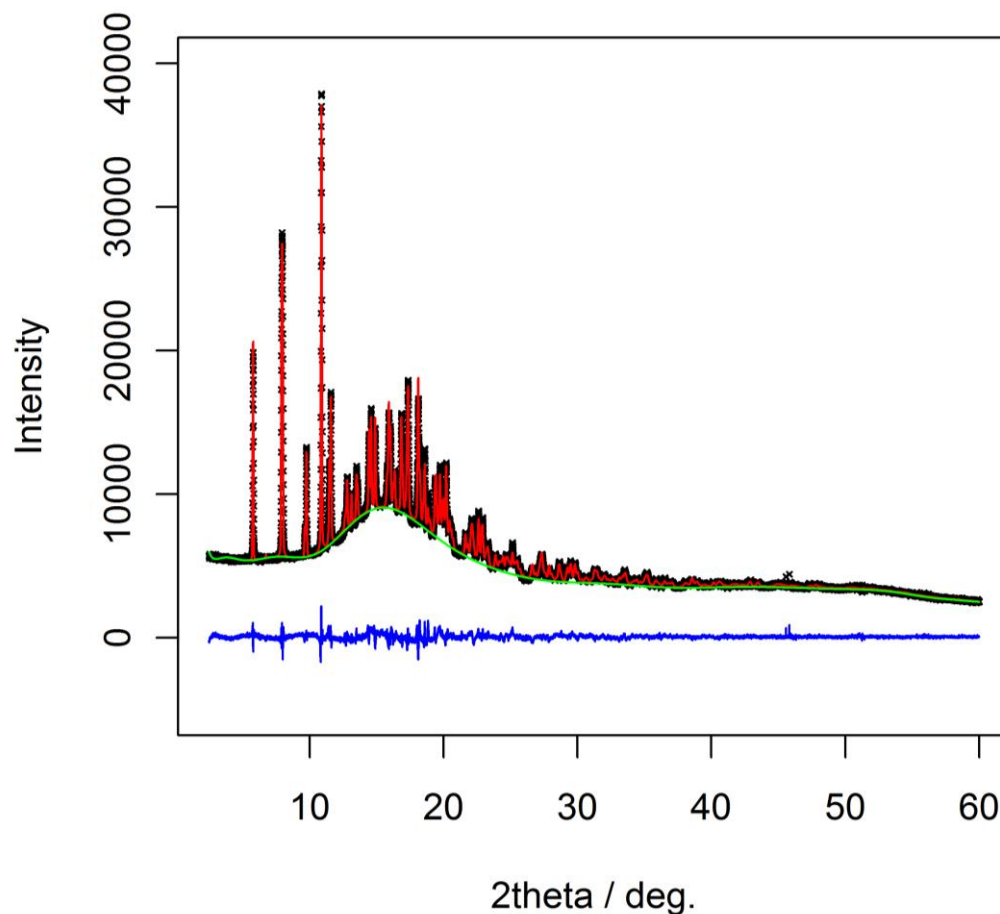


Figure S17. Final Rietveld refined pattern (calculated intensity, red), experimental data (black) for **LM+12.(ACON)** and difference $I_{\text{calc}} - I_{\text{exp}}$. (blue).

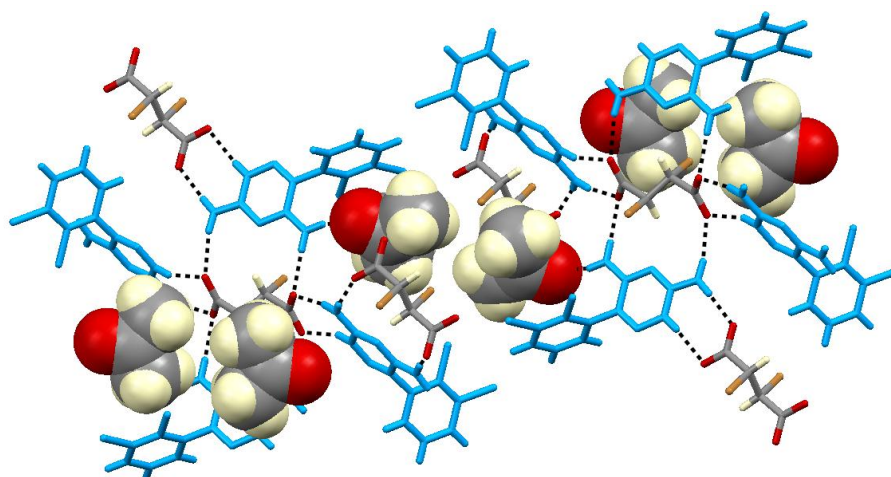


Figure S18. The crystal packing diagram of **LM+12.(ACON)** structure showing the two main hydrogen-bonded ring synthons of type $R_2^2(8)$ and $R_2^2(13)$ between the **LM** (in blue) and **12** molecules. The ACN guest molecules (drawn in spacefill mode) are filling the cavities limited by the dichlorophenyl and triazine groups of the **LM** and the central carbon backbone of the acid **12**.

Section 3. Infrared spectroscopy

Fourier transform infrared (FTIR) spectra of samples were collected in the mid-IR region with a ThermoNicolet Nexus spectrometer equipped with a Smart Golden Gate Attenuated Total Reflection (ATR) accessory.

The FTIR-ATR spectra of powder samples of all the LAG synthesized LMDC-G compounds are characterized by the presence of broad bands between 3300 and 2200 cm^{-1} , corresponding to stretching vibrations of N-H^+ of amine hydrogen bonded salts, and also by the shifting to lower frequencies of the C=O characteristic band of the dicarboxylic acid, which indicates the carboxylate anion formation¹. Moreover the FTIR-ATR depict the solvent guest molecule content showing the characteristic bands corresponding to the guest molecules included in each particular case. (see Tables S19 to S22)

1. Silverstein, R. M. & Webster, F. X. *Spectrometric Identification of Organic Compounds*, 6th ed. Wiley, New York, 1998; Chapter 3, pp 71-143.

Table S19. Table with the FTIR-ATR selected characteristic bands together with the FTIR-ATR spectra for all the isostructural **LM+DC**.(DMSO) LAG synthesized compounds (cm^{-1}).

LMDC-Guest Compound	Included guest bands (DMSO)	Hydrogen bonded $\text{N}^{(+)}\text{-H}$ bands	C=O shifted bands of $\text{COO}^{(-)}$	C=O bands of the COOH groups in the neutral DC
LM+1 .(DMSO)	1330, 1039, 800	3230, 3039	1667	1677
LM+2 .(DMSO)	1369, 1022, 799	3246, 2993	1666	1658
LM+3 .(DMSO)	1374, 1058, 800	3230, 2952	1658	1678
LM+4 .(DMSO)	1356, 1013, 799	3218, 2979	1669	1732
LM+5 .(DMSO)	1355, 1013, 798	3164, 2975	1669	1713
LM+6 .(DMSO)	1382, 1012, 799	3241, 2987	1672	1690
LM+7 .(DMSO)	1379, 1011, 799	3159, 2992	1668	1690
LM+8 .(DMSO)	1378, 1041, 801	3228, 2995	1664	1681
LM+9 .(DMSO)	1377, 1039, 798	3242, 3015	1665	1697
LM+10 .(DMSO)	1370, 1035, 798	3226, 2993	1654	1688
LM+11 .(DMSO)	1355, 1056, 804	3284, 3048	1650	1760, 1709
LM+12 .(DMSO)	1366, 1041, 795	3249, 3050	1662	1696

The figure displays 12 stacked FTIR-ATR spectra, one for each compound from LM+1 to LM+12. The x-axis represents Wavenumbers (cm^{-1}) ranging from 4000 to 500, and the y-axis represents Percent Transmittance (%T) ranging from 50 to 100. Each spectrum shows characteristic absorption bands, with the most prominent ones corresponding to the values listed in Table S19. The spectra are vertically offset for clarity, with the top spectrum (LM+1) starting at 100%T and the bottom spectrum (LM+12) starting at 50%T.

Table S20. Table with the FTIR-ATR selected characteristic bands together with the FTIR-ATR spectra for all the isostructural **LM+DC**.(ACON) LAG synthesized compounds (cm^{-1}).

LMDC-Guest Compound	Included guest bands (Acetone)	Hydrogen bonded $\text{N}^{(+)}\text{-H}$ bands	C=O shifted bands of $\text{COO}^{(-)}$	C=O bands of the COOH groups in the neutral DC
LM+1 .(ACON)	1711	3372, 3046, 2712	1644	1677
LM+2 .(ACON)	1712	3310, 3127, 2702	1656	1658
LM+3 .(ACON)	1697	3367, 3250, 2960	1658	1678
LM+4 .(ACON)	1709	3305, 2988, 2726	1651	1732
LM+5 .(ACON)	1711	3335, 3005, 2721	1651	1713
LM+6 .(ACON)	1711	3357, 3000, 2737	1658	1690
LM+7 .(ACON)	1712	3358, 3001, 2742	1659	1690
LM+8 .(ACON)	1712	3013	1654	1681
LM+9 .(ACON)	1710	3010	1647	1697
LM+10 .(ACON)	1711	3059	1647	1688
LM+12 .(ACON)	1710	3308,3043	1655	1696

Table S21. Table with the FTIR-ATR selected characteristic bands together with the FTIR-ATR spectra for all the isostructural **LM+DC**.(THF) LAG synthesized compounds (cm^{-1}).

LMT-DCA-Guest Compound	Included guest bands (THF)	Hydrogen bonded $\text{N}^{(+)}\text{-H}$ bands	C=O shifted bands of $\text{COO}^{(-)}$	C=O bands of the COOH groups in the neutral DC
LM+1 .(THF)	1051, 994	3067	1652	1677
LM+2 .(THF)	1051, 990	3269, 2976	1661	1658
LM+3 .(THF)	1038, 957	3139, 3056, 2916	1655	1678
LM+4 .(THF)	1059, 984	3268, 3065, 2973	1658	1732
LM+5 .(THF)	1061, 975	3334, 3054, 2831	1650	1713
LM+8 .(THF)	1058, 986	3039, 2873	1653	1681

Table S22. Table with the FTIR-ATR selected characteristic bands together with the FTIR-ATR spectra for all the isostructural **LM+DC**.(ACRO) LAG synthesized compounds (cm^{-1}).

LMDC-Guest Compound	Included guest bands (Acroleine)	Hydrogen bonded $\text{N}^{(+)}\text{-H}$ bands	C=O shifted bands of $\text{COO}^{(-)}$	C=O bands of the COOH groups in the neutral DC
LM+1 .(ACRO)	1687, 977	3064	1654, 1578	1677
LM+8 .(ACRO)	1686, 971	3064	1583, 1538	1681
LM+9 .(ACRO)	1688, 970	3122	1581, 1536	1697
LM+10 .(ACRO)	1687, 971	3134	1646, 1578, 1540	1688

The figure displays four stacked FTIR-ATR spectra for the compounds LM+1.(ACRO), LM+8.(ACRO), LM+9.(ACRO), and LM+10.(ACRO). The x-axis represents Wavenumbers (cm^{-1}) ranging from 4000 to 1000, and the y-axis represents Transmittance (%T) ranging from 60 to 100. Each spectrum shows characteristic absorption bands, with the most prominent ones occurring between 1600 and 1700 cm^{-1} , corresponding to the C=O stretching vibrations mentioned in the table above.

Section 4. Thermal analyses

Differential scanning calorimetric (DSC) analyses were performed using a Mettler Toledo DSC822e unit. The samples (2–5 mg) were encapsulated in 40 μL aluminium crucibles with pierced lids. Heating rates of $10\text{ }^\circ\text{C min}^{-1}$ and nitrogen purge at 80 mL min^{-1} were employed for the temperature range 25–325 $^\circ\text{C}$. The mass loss of the sample as a function of temperature (TGA) was determined using a Mettler Toledo TGA/SDTA851e unit. The samples were placed in 100 μL aluminium crucibles and heated from 25 to 325 $^\circ\text{C}$ at $10\text{ }^\circ\text{C min}^{-1}$. Nitrogen purge at 80 mL min^{-1} was employed.

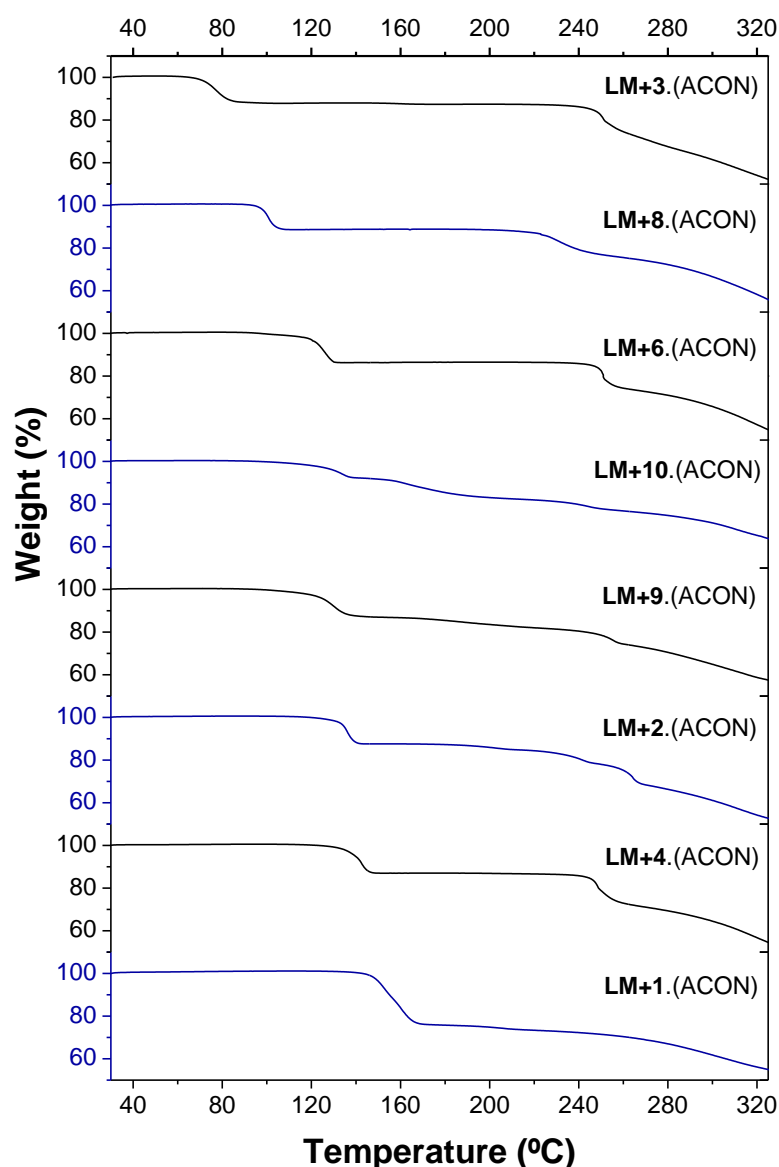


Figure S23. Differences on thermal stability of **LM+DC.(ACON)** isostructural compounds depending on the DC forming the host are shown by TGA analyses. The temperature of solvent guest release compounds shows temperature ranging from an onset of 150 $^\circ\text{C}$ for the most stable **LM+1.(ACON)** to an onset of 70 $^\circ\text{C}$ for the most unstable **LM+3.(ACON)**.

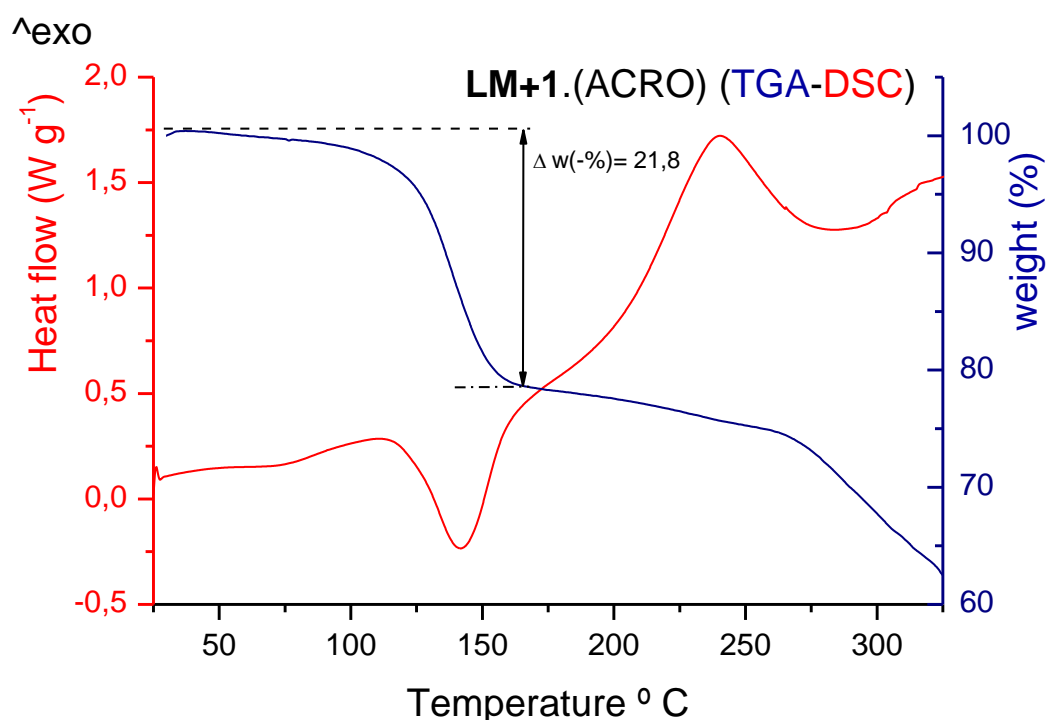


Figure S24. DSC-TGA of the **LM+1.(ACRO)** showing an initial weight loss in the TGA of 21.8 % corresponding to the 21.2 % theoretical weight loss of three ACRO guest molecules calculated for an stoichiometry of 2:1:3 (LM : 1 : ACRO).

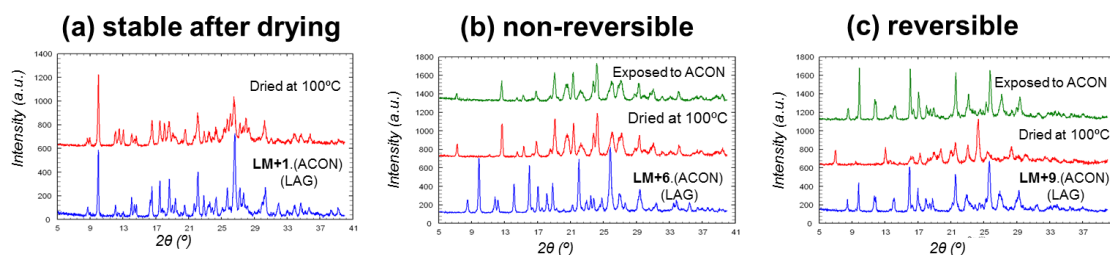


Figure S25. Reversibility of guest inclusion in LM+DC.(guest). (a) Stable behaviour of the **LM+1.(ACON)** compound shown by no changes in the PXRD pattern after drying of the sample at 100°C; (b) non-reversible desolvation of **LM+6.(ACON)** shown by the formation of the crystalline phase collapsed LM+6 upon drying and no conversion of this guest-free phase upon exposure to ACON vapours and (c) reversible desolvation of **LM+9.(ACON)** shown by the formation of crystalline collapsed **LM+9** after drying followed by the re-formation of **LM+9.(ACON)** after exposure to ACON vapour.

Section 5. Computational methods

In order to rationalise formation and compare isostructural solvated salts of **LM** with **DC** and guest molecules, systems were modelled in such a way that **LM** and **DC** were adapted from the experimentally determined crystal structures of **LM+1.(DMSO)**, **LM+2.(DMSO)** and **LM+3.(DMSO)** and the hydrogen atoms were optimised on an isolated molecule calculation, whereas guest solvent molecules were built from scratch and then fully optimised to allow generating a large set of hypothetical solvated salt structures. Next, known solvent molecules were exchanged in **LM+DC.(DMSO)** systems by fully optimised solvent molecules. Molecular optimisation was performed within Gaussian03¹ using the B3LYP functional and 6-31G** basis set.

The crystal structure of **LM+1.(DMSO)** consists of LM1, and two solvent molecules; DMSO occupying 20% and THF occupying 80% of the solvent accessible volume. In order to model LM1.(DMSO), 100% DMSO occupancy was imposed on the **LM+1.(DMSO)** crystal structure.

The W99 potential^{2, 3} was used to represent repulsion – dispersion contributions to the intermolecular potential and interactions were summed to a 15Å cutoff. Atomic multipoles were used to represent electrostatic contributions to the intermolecular potential. Atomic multipoles up to hexadecapole on each atom were generated via a Distributed Multipole Analysis (DMA)⁴ of a B3LYP/6-31G** electron density using the program GDMA. All charge-charge, charge-dipole, and dipole-dipole contributions to the lattice energy were evaluated using the Ewald summation, while higher order electrostatic interactions (up to R^{-5}) were summed to a 15 Å cutoff on entire molecules. Lattice energy minimisations of structures were performed using the DMAREL program.⁵ All structures were minimised with respect to the position and orientation of the molecules and the size and shape of the unit cell. The molecular positions and conformations were treated as rigid during lattice energy minimisations and the centre of the interaction for hydrogen atoms was shifted by 0.1 Å along the X-H bond (X=C, N, O) towards the heavy atom after molecular optimisation. Quantitative analysis of percentage filled space (PI) and accessible volumes were performed using calculations within Platon (1.2 Å probe radius and 0.2 Å grid step) and voids were visualised using Mercury. Molecular volumes of solvents were calculated using the methodology developed by Molinspiration.⁶

1. Frisch, M. J. *et al. Gaussian 03, Revision B.03.* (Gaussian, Inc., 2004).
2. Williams, D. E. Improved intermolecular force field for crystalline hydrocarbons containing four- or three-coordinated carbon. *Journal of Molecular Structure* **485**, 321-347 (1999).
3. Williams, D. E. Improved intermolecular force field for molecules containing H, C, N, and O atoms, with application to nucleoside and peptide crystals. *Journal of Computational Chemistry* **22**, 1154-1166 (2001).
4. Stone, A. J. Distributed multipole analysis, or how to describe molecular charge-distribution. *Chemical Physics Letters* **83**, 233-239 (1981).
5. Price, S. L., Willock, D. J., Leslie, M. & Day, G. M. *DMAREL.* (2001).
6. *Molinspiration*, <http://molinspiration.com/services/volume.html>

Table S26. Lattice parameters of the experimentally determined **LM+DC**.(DMSO) structures and the lattice energy minimized empty framework structures.

System name	<i>a</i> [Å]	<i>b</i> [Å]	<i>c</i> [Å]	α [°]	β [°]	γ [°]
LM+1 .(DMSO) exp	11.08	10.32	16.31	90.00	108.64	90.00
LM+1	10.78	10.22	16.30	90.00	108.53	90.00
LM+2 .(DMSO) exp	10.85	10.92	15.88	90.00	109.06	90.00
LM+2	10.72	10.82	15.99	90.00	110.29	90.00
LM+3 .(DMSO) exp	11.19	10.71	15.98	90.00	109.35	90.00
LM+3	11.08	10.73	15.77	90.00	107.22	90.00

Table S27. Difference in calculated lattice energy between all modeled **LM+DC**.(guest) salts and the empty **LM+DC** framework [$E_{\text{latt}}(\text{LM+DC}(\text{guest})) - E_{\text{latt}}(\text{LM+DC})$]. All energies are in kJ/mol and correspond to the inclusion of 2 guest molecules in each cavity (providing a 2:1:2 **LM:DC:guest** stoichiometry).

	DMSO	ACON	THF	ACRO
LM+1	-106.5	-86.4	-83.0	-80.2
LM+2	-105.5	-87.6	-83.2	-80.2
LM+3	-113.3	-87.4	-86.5	-80.1